Helium-induced electronic transitions in photo-excited Ba⁺–He_n exciplexes

Patricia Vindel Zandbergen,[1,a)] Manuel Barranco,[1,2,3] Fausto Cargnoni,[4,b)]
Marcel Drabbels,[5,c)] Martí Pi,[2,3] and Nadine Halberstadt[1,d)]

[1]*Laboratoire Collisions Agrégats Réactivité (LCAR), IRSAMC, Université de Toulouse, CNRS UMR 5589,
Toulouse, France*
[2]*Departament FQA, Facultat de Física, Universitat de Barcelona, Barcelona, Spain*
[3]*Institute of Nanoscience and Nanotechnology (IN2UB), Universitat de Barcelona, Barcelona, Spain*
[4]*CNR–ISTM, Via Golgi 19, 20133 Milano, Italy*
[5]*Laboratory of Molecular Nanodynamics, Swiss Federal Institute of Technology Lausanne (EPFL),
CH-1015 Lausanne, Switzerland*

The possibility for helium-induced electronic transitions in a photo-excited atom is investigated using Ba⁺ excited to the 6p ^{2}P state as a prototypical example. A diabatization scheme has been designed to obtain the necessary potential energy surfaces and couplings for complexes of Ba⁺ with an arbitrary number of helium atoms. It involves computing new He–Ba⁺ electronic wave functions and expanding them in determinants of the non-interacting complex. The 6p ^{2}P ← 6s ^{2}S photodissociation spectrum of He···Ba⁺ calculated with this model shows very weak coupling for a single He atom. However, several electronic relaxation mechanisms are identified, which could potentially explain the expulsion of barium ions from helium nanodroplets observed experimentally upon Ba⁺ photoexcitation. For instance, an avoided crossing in the ring-shaped He₇Ba⁺ structure is shown to provide an efficient pathway for fine structure relaxation. Symmetry breaking by either helium density fluctuations or vibrations can also induce efficient relaxation in these systems, e.g., bending vibrations in the linear He₂Ba⁺ excimer. The identified relaxation mechanisms can provide insight into helium-induced non-adiabatic transitions observed in other systems. *Published by AIP Publishing.*
https://doi.org/10.1063/1.5022863

I. INTRODUCTION

In recent years, great progress has been made in the study of impurity atoms and ions in cold helium environments, from solid to superfluid bulk ^{4}He to ^{4}He nanodroplets and cryogenic ^{4}He gas.[1–12] One fascinating result of these studies has been the evidence that exciplexes can be formed upon photoexcitation of alkali metal atoms. These molecular complexes formed by an alkali atom in an excited state, typically np state, and one or several ground state He atoms, have been first invoked to explain the quenching of laser-induced fluorescence of light alkalis in liquid and solid helium.[13,14] This was demonstrated for Rb in pressurized liquid He.[15] As reviewed in Ref. 9, they have also been studied from the theoretical point of view. The photoinduced dynamics of excited alkalis have later been extensively investigated using superfluid He nanodroplets; see Ref. 11 for a review. The weakly interacting alkali atoms are known to reside in a dimple at the surface of these droplets. The photoexcitation of the surface located atoms usually leads to their desorption and is often accompanied by exciplex formation.[16–34]

Positive alkali earth ions have an electronic structure similar to that of alkali atoms, but their charge makes their interaction with helium more attractive and they tend to be more solvated. This makes them very interesting systems to study the influence of helium-induced relaxation on the photoexcitation dynamics. In Ba⁺, this process was first observed in a spectroscopic study of 6p ^{2}P Ba⁺ in liquid, superfluid helium by Reyher *et al.*[35] They observed three emission bands, 6s ^{2}S$_{1/2}$ ← 6p ^{2}P$_{1/2}$ and 5d ^{2}D ← 6p ^{2}P$_{1/2}$ emission from the 6p ^{2}P$_{1/2}$ "bubble state" and the third one unassigned. Since both assigned emissions were identical upon D1 (6p ^{2}P$_{1/2}$) or D2 (6p ^{2}P$_{3/2}$) excitation, it implied that the 6p ^{2}P$_{3/2}$ state had relaxed to 6p ^{2}P$_{1/2}$ before fluorescing.

Upon D2 line excitation in cold He gas (T = 3–25 K), Fukuyama *et al.*[36,37] observed a sharp emission line at the D1 transition and a broad fluorescence band in the range of 20 500–21 800 cm^{-1} (488-459 nm). The D1 line intensity was attributed to fine structure relaxation of the He–Ba⁺ (6p ^{2}Π$_{3/2}$) exciplex by collision with another helium atom. The broadband emission was assigned to direct fluorescence from excited vibrational levels of the He···Ba⁺ 6p ^{2}Π$_{3/2}$ complex.

This study was completed at lower temperature (T = 1.35–1.7 K) by Moroshkin and Kono.[38] As in the preceding study, they have observed a broad band corresponding to exciplex emission from a population of vibrationally excited levels of

a)Electronic mail: Patricia.Vindel@irsamc.ups-tlse.fr
b)Electronic mail: fausto.cargnoni@istm.cnr.it
c)Electronic mail: marcel.drabbels@epfl.ch
d)Electronic mail: Nadine.Halberstadt@irsamc.ups-tlse.fr

the 6p $^2\Pi_{3/2}$ state, as confirmed by a theoretical simulation using the high accuracy potential energy curves of Mella and Cargnoni.[39] In addition, two lines originating from the 6p $^2P_{1/2}$ state were assigned to collisional fine structure relaxation, either in the atom or in the exciplex.

Recently, spectroscopic experiments on the 6p $^2P \leftarrow$ 6s ^2S transition on Ba$^+$ in helium nanodroplets have concluded that the barium ion is solvated near the center of the droplet,[40] based on the comparison with the corresponding transition in liquid helium. Excitation of the 6p ^2P states makes for a very interesting test case for studying photoexcitation dynamics since a competition is expected between desorption and rearrangement of the surrounding helium about the excited state orbital. From the analysis of the time-of-flight mass spectra, it was concluded that the barium ions were ejected from the helium droplets as Ba$^+$ or Ba$^+$He$_n$, a process that had been predicted for neon cluster ionization[41,42] and observed for molecular ions.[40,43]

Analysis of the results from mass spectra and velocity map imaging revealed that fine structure relaxation cannot be complete. For instance, Ba$^+$ or He$_n$Ba$^+$ ions were ejected but their translational temperature depended on the initially excited state, with a maximum of 178 ± 4 K for bare Ba$^+$ ions upon D1 excitation and a leveling off around ~60 K for He$_n$Ba$^+$ for increasing n. Also, the ejected Ba$^+$ velocity was much higher than the Landau critical velocity, showing that the desolvation mechanism differs from that of Ag.[27]

Mella and Cargnoni have performed a diffusion Monte Carlo (DMC) study of the relative stability of He$_n$Ba$^+$ ^2P exciplexes, using a diatomics in molecules (DIM) model Hamiltonian built from high accuracy *ab initio* potential energy curves for He$\cdots$Ba$^+$ combined with an atomic model for the spin-orbit interaction. As expected from the shape of the 6p $^2\Pi_{3/2}$ orbital, the first two helium atoms for this state are strongly bound in a linear configuration at a distance of ~3 Å from Ba$^+$, additional atoms being more loosely bound at larger distances (~6 Å). The energetics are more complex for the 6p $^2P_{1/2}$ state, with an alternance of weak van der Waals bonds at ~7 Å (1st and 3rd atoms) and strong bonds around ~3.2 Å similar to those found in alkali exciplexes ($n = 2$ adopts a linear configuration with an evaporation energy of 250.3 cm^{-1}, $4 \leq n \leq 7$ a ring structure in a plane around the Ba$^+$ ion). The authors propose He$_2$Ba$^+$ 6p $^2P_{1/2}$ emission to the ground state as the origin of the unknown band at 523 nm (19 121 cm^{-1}) in the Ba$^+$ fluorescence spectrum in superfluid helium.[35] However, it should be accompanied by emission to the $^2D_{3/2}$ state which was not observed.

More recently Leal *et al.*[44] have used helium time-dependent density functional theory (He-TDDFT) to characterize the dynamics following photoexcitation of Ba$^+$ 6p ^2P in ^{4}He droplets. The experimental excitation spectrum was well reproduced using Mella and Cargnoni's He–Ba$^+$ interaction energy curves.[39] But due to the rather deep He–Ba$^+$ 6p $^2\Pi_{3/2}$ potential well, excitation did not lead to ejection of the Ba$^+$ ion, in contrast to what experiments suggest. Even assuming formation of an exciplex followed by fluorescence decay to the repulsive part of the He–Ba$^+$ interaction in the 5d $^2D_{3/2}$ or 6s $^2S_{1/2}$ states, Ba$^+$ remained inside the droplet due to the deep attraction in the final states. Therefore another mechanism has

to be invoked in order to explain the ejection of Ba$^+$, with or without helium atoms attached.

The purpose of this study is to investigate the possibility for electronic relaxation induced by helium in an excited atom. We design a diabatization procedure which then allows us to describe the potential energy surfaces and couplings required to study this process with an arbitrary number of helium atoms (Sec. II). We first simulate the photodissociation spectrum of Ba$^+$ excited to the 6p ^2P valence band, which is simple enough to be amenable to high quality *ab initio* calculations (Sec. III), in order to check that our model gives excited state lifetimes compatible with the experimental observation of He$\cdots$Ba$^+$ excimers (Sec. IV). We then turn to explore the possibility for helium-induced transitions in He$_n$Ba$^+$ configurations involving more helium atoms: linear $n = 2$ and ring $n = 7$ bubble states or exciplexes (Sec. V). Finally, we summarize the key results and propose outlooks of this work (Sec. VI).

II. ELECTRONIC STRUCTURE AND DIABATIZATION

A. Determination of the He$\cdots$Ba$^+$ electronic structure

We first determined *ab initio* potential energy curves for He$\cdots$Ba$^+$ by solving the spin-free electronic Hamiltonian in the basis of asymptotic (i.e., non-interacting) ground- and excited-state determinants of the complex. Interaction energies at finite distances are the same as the ones obtained previously.[39,45] In addition, the present setting makes it possible to write the He$\cdots$Ba$^+$ electronic Hamiltonian in the form of a diabatic Hamiltonian including all the 6s ^2S, 5d ^2D, and 6p ^2P electronic states and their couplings (diabatization).

In the present section, we briefly summarize the method used to determine them, focusing on the new points relevant to the present investigation. The interested reader is referred to Refs. 39 and 45 for more details.

We recall here that the computations described below neglect spin-orbit effects, which are included *a posteriori* as discussed in Sec. II C. The physics of the He$\cdots$Ba$^+$ dimer is quite simple. The ground state potential is essentially dominated by the dispersion interaction between helium and the outermost electron of the ion, whose reference wave function is well described by a single determinant. Minor contributions to the interaction also come from the inner electron shells of barium. The coupled cluster approach at the CCSD(T) level (inclusion of single, double, and perturbative triple excitations) adopted in conjunction with high-quality basis sets and a pseudopotential for the 46 core electrons of the metal atom, proved adequate to recover an accurate interaction potential.[45] To provide a reliable description of the excited He$\cdots$Ba$^+$ system, we first performed test computations on the isolated Ba$^+$ ion. We adopted a Configuration Interaction (CI) strategy and included in the final wave function up to triple excitations, correlating the 9 outermost electrons (i.e., the two external shells) of Ba$^+$.[39] Each one among the lowest ^2P and ^2D states is dominated by just one single excited determinant, accounting for the promotion of the outermost unpaired 6s electron to the p or the d shells. Further tests proved that this elementary behavior holds true also upon interaction with helium, even at highly repulsive He$\cdots$Ba$^+$ conformations. The final

wave function for He$\cdots$Ba$^+$ was therefore built according to a multi-reference configuration interaction scheme. The promotion of the outermost electron of barium into excited states is accounted for by the multiple reference, whose active space is extended up to the 6p and 5d shells. Intramonomer correlation and dispersion interaction between Ba$^+$ and He has been accounted for by including single and double excitations starting from an active space of 11 electrons: the 1s^2 pair of He plus 9 electrons coming from Ba$^+$ (5s^2, 5p^6 plus the outermost shells electron). Perturbative computations[44] proved this variational scheme to be well grounded. Interaction energies and wave functions have been computed at 33 internuclear distances ranging from 1.5 to 10.0 Å, plus the asymptote at 100.0 Å, sampling more finely the regions where the potential energy surfaces undergo sudden changes.

In order to estimate the perturbation induced by helium onto the electronic structure of the ion, for all internuclear separations the eigenvectors of the dimer have been projected onto the asymptotic ones (computed at the distance of 100.0 Å at the same level of theory), which closely mimic the excitations of the unperturbed Ba$^+$ monomer. Due to symmetry, the interaction with helium can induce mixing only between Ba$^+$ states with the same value of Λ, the projection of the Ba$^+$ orbital electronic angular momentum on the internuclear axis z. This defines the subsets Σ ($\Lambda = 0$), where 6s, 6p$_z$, and 5d$_{z^2}$ are mixed; Π ($\Lambda = \pm 1$), where 6p$_x$ and 5d$_{xz}$ or 6p$_y$ and 5d$_{yz}$ are mixed; and Δ ($\Lambda = \pm 2$), where 5d$_{xy}$ and 5d$_{x^2-y^2}$ are mixed (the Ba$^+$ states are labeled here by the outermost unpaired electron orbital). As can be seen in Fig. 1, the eigenstate coefficients change very smoothly with the internuclear separation, and

the mixing remains quantitatively quite small but for highly repulsive dimer conformations at short distances.

B. Diabatization: He···Ba$^+$ electronic Hamiltonian with He-induced couplings

The electronic states considered here are the lowest excited states with principal quantum number $n = 5$ or 6: 5d ^{2}D or 6p ^{2}P; and the ground electronic state is 6s ^{2}S.

The Hamiltonian for the system is given by

$$H = H_M + H_{SO} \quad \text{with} \quad H_M = H_{el}(R) + T_{\mathbf{R}}, \qquad (1)$$

where $\mathbf{R}$ is the distance vector from Ba$^+$ to He and R its modulus; H_M is the molecular Hamiltonian, which is the sum of the electronic Hamiltonian $H_{el}(R)$ for a fixed value of R and the kinetic energy operator $T_{\mathbf{R}}$ for the nuclei; and H_{SO} is the spin-orbit Hamiltonian.

In this section, we describe the electronic Hamiltonian H_{el} used to take into account transitions between electronic states of Ba$^+$ due to the presence of a helium atom ("non-adiabatic transitions" or "internal conversion" or "electronic relaxation"). Spin-orbit couplings due to H_{SO} are discussed in Sec. II C.

In the electronic structure calculation presented in Sec. II A, H_{el} is expanded in a common basis set of isolated Ba$^+$ determinants for all distances, denoted here as $|nL\Lambda\rangle$, and then diagonalized (L denotes the electronic orbital angular momentum quantum number and Λ denotes the one for its projection onto the He–Ba$^+$ axis). The corresponding eigenstates $|\widetilde{\varphi}_k\rangle$ of H_{el} with eigenvalues $\widetilde{V}_k(R)$ will be referred to here as *adiabatic*,

$$H_{el} |\widetilde{\varphi}_k\rangle = \widetilde{V}_k(R) |\widetilde{\varphi}_k\rangle, \qquad (2)$$

$$|\widetilde{\varphi}_k\rangle = \sum_n \sum_L \sum_\Lambda \widetilde{M}_{nL\Lambda,k}(R) |nL\Lambda\rangle. \qquad (3)$$

The $\widetilde{V}_k(R)$ are the adiabatic potential energy curves for the He–Ba$^+$ interaction in different electronic states, i.e., H_{el} is diagonal at each value of R. However, since the eigenvectors $|\widetilde{\varphi}_k\rangle$ depend parametrically on R, they can be coupled by the kinetic term $T_{\mathbf{R}}$ of the nuclei, therefore inducing transitions between Ba$^+$ electronic states. These kinetic couplings, also called "non-adiabatic" couplings, are computationally difficult to treat because they can exhibit steep variations. Here we describe a *diabatization* approach to describe transitions between Ba$^+$ electronic states without having to deal with kinetic couplings. The price to pay is that the electronic Hamiltonian is no longer diagonal, but its diagonalization gives back the adiabatic potential energy curves.

A *diabatic* representation of the Hamiltonian can be obtained by transforming the (diagonal) matrix $\widetilde{\mathbf{V}}$ of the $\widetilde{V}_k(R)$ adiabatic potential energy curves to the initial $\{|nL\Lambda\rangle\}$ basis set using the matrix $\widetilde{\mathbf{M}}$ of the coefficients defined in Eq. (3),

$$\mathbf{V} = \widetilde{\mathbf{M}}\widetilde{\mathbf{V}}\widetilde{\mathbf{M}}^{-1}. \qquad (4)$$

This representation is perfectly diabatic, i.e., the kinetic couplings are zero, because the basis set used in Sec. II A for electronic structure calculation does not depend on R.

FIG. 1. Coefficients of the 6s (black curve, □), 5d$_{z^2}$ (blue curve, ×), and 6p$_z$ (purple curve, +) unperturbed Ba$^+$ monomer states for the Σ eigenstates 1Σ (bottom, mostly 6s), 2Σ (middle, mostly 5d$_{z^2}$), and 3Σ (top, mostly 6p$_z$) states of He$\cdots$Ba$^+$ as a function of internuclear distance. [The Ba$^+$ states are labeled here by the outermost unpaired electron orbital. The coefficients correspond to the $\Lambda = 0$ $\widetilde{M}_{nL\Lambda,k}(R)$ coefficients defined in Eq. (3).]

Because the configuration interaction of the electronic structure calculations involved more terms than the minimal set consisting of the 6s ^{2}S, 5d ^{2}D, and 6p ^{2}P states of interest here, we truncate the expansion in Eq. (3) to the minimum basis set, which on the other hand contains the largely dominant terms.

In order to make the resulting truncated matrix **M** orthonormal, the (truncated) vectors are renormalized and orthogonalized using Schmidt orthogonalization.[46] The final adiabatic basis set is then defined by

$$|\varphi_k\rangle = \sum_{k'=1}^{9} M_{k',k}(R) |k'\rangle, \qquad (5)$$

where $|\varphi_k\rangle$, $k = 1$–9, are the truncated and orthogonalized eigenvectors and $|k'\rangle$, $k' = 1$–9, are the asymptotic eigenvectors of the dimer mimicking the ground and excited states of isolated Ba$^+$ and corresponding to effective 1-electron orbitals 6s, 6p$_x$, 6p$_y$, 6p$_z$, 5d$_{yz}$, 5d$_{z^2}$, 5d$_{xz}$, and 5d$_{x^2-y^2}$ as described at the end of Sec. II A. The reduced size diabatic electronic Hamiltonian matrix **W** is then obtained as

$$\mathbf{W} = \mathbf{M}\widetilde{\mathbf{W}}\mathbf{M}^{-1}, \qquad (6)$$

where $\widetilde{\mathbf{W}}$ denotes the truncated $\widetilde{\mathbf{V}}$ diagonal matrix of the potential energy curves.

As noted at the end of Sec. II A, Λ is a good quantum number because of cylindrical symmetry. As a result, only subsets of electronic states with the same value of Λ are coupled. Figure 2 shows the resulting diabatic potential energy curves
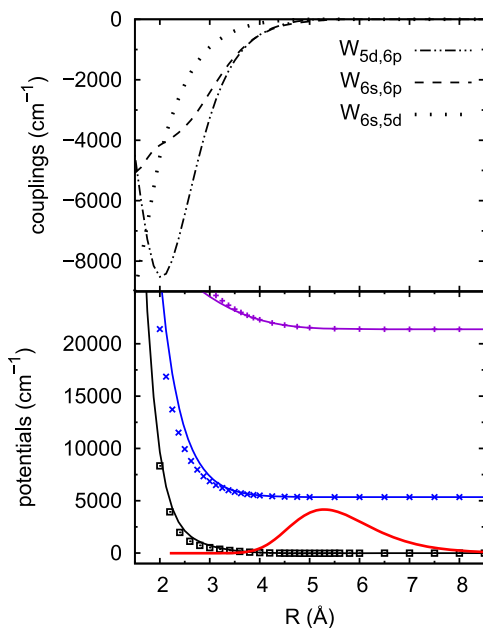
FIG. 2. Σ ($\Lambda = 0$) diabatic potential energy curves and couplings obtained from the diabatization procedure described in Sec. II B. Bottom plot: □ (black): *ab initio* $\widetilde{V}_{6s}(R)$; × (blue): *ab initio* $\widetilde{V}_{5d_{z^2}}(R)$; + (purple): *ab initio* $\widetilde{V}_{6p_z}(R)$. Solid lines: $W_{6s,6s}(R)$ (black), $W_{5d_{z^2},5d_{z^2}}(R)$ (blue), and $W_{6p_z,6p_z}(R)$ (purple) *diabatic* potentials defined as the diagonal elements of W corresponding to $\Lambda = 0$ in Eq. (6). The ground bound state wave function is plotted in red to visualize the Franck-Condon region. Top plot: Couplings between Σ states, i.e., off-diagonal elements $W_{5d_{z^2},6p_z}(R)$ (double dotted-dashed); $W_{6s,6p_z}(R)$ (dashed); and $W_{6s,5d_{z^2}}(R)$ (dotted) in Eq. (6).

and couplings compared to the original *ab initio* curves for $\Lambda = 0$. As expected, the couplings are stronger in the repulsive region of the adiabatic curves. The $\Lambda = \pm 1$ diagonal diabatic curves are very close to the adiabatic ones and the couplings are rather small. There are only two $\Lambda = \pm 2$ curves, both corresponding to d states, and they remain uncoupled.

C. Spin-orbit Hamiltonian

We use the common assumption that spin-orbit interaction can be approximated by

$$H_{SO} = g_{nL} \mathbf{L} \cdot \mathbf{S} = \frac{1}{2} g_{nL} (\mathbf{J}^2 - \mathbf{L}^2 - \mathbf{S}^2). \qquad (7)$$

It couples the electronic orbital angular momentum **L** and electronic spin **S** of Ba$^+$ to form the total electronic angular momentum **J**. The spin-orbit coupling constants g_{nL} are extracted from the asymptotic spin-orbit splittings of Ba$^+$: g_{6P} = $(2/3\hbar^2) \Delta_{SO}(6p\ ^2P)$ and $g_{5D} = (2/5\hbar^2) \Delta_{SO}(5d\ ^2D)$. We have used the values of the atomic state energies[47] to calculate Δ_{SO}: $E(5d\ ^2D_{3/2}) = 4873.852$ cm^{-1}; $E(5d\ ^2D_{5/2}) = 5674.807$ cm^{-1}; $E(6p\ ^2P_{1/2}) = 20\ 261.561$ cm^{-1}; $E(6p\ ^2P_{3/2}) = 21\ 952.404$ cm^{-1}. The basis set of $\{|k\rangle\}$ orbitals [Eq. (5) in Sec. II B] is doubled to include the two possible projections $\pm 1/2$ of the electronic spin, $\{|K\rangle\}$, $K = 1$–18, resulting in doubly degenerate eigenstates (Kramer's pairs) for the total Hamiltonian, Eq. (1),

$$\psi_K = \sum_{K'=1}^{18} c_{K'K} |K'\rangle, \quad K = 1, 18. \qquad (8)$$

Two different basis sets and spectroscopic notations are used in this work. The first one is Hund's case (a) or uncoupled basis set $|n, L, \Lambda, S, \Sigma\rangle$, where Λ and Σ are the projections of **L** and **S** onto the interatomic axis, respectively. The second one is Hund's case (c) or coupled basis set, which is asymptotically the basis set of the atomic eigenstates, $|n, L, S, J, \Omega\rangle$, where $\mathbf{J} = \mathbf{L} + \mathbf{S}$ and $\Omega = \Lambda + \Sigma$ is the projection of **J** onto the interatomic axis (note that Ω is a good quantum number for both the electrostatic and the spin-orbit Hamiltonian in cylindrical symmetry). At short distances where the energy difference between states with same L but different values of Λ is larger than the spin-orbit splitting, the eigenstates can be labeled using case (a) notation $^{2S+1}\Lambda_\Omega$. For instance, the states originating from Ba$^+$ (6p ^{2}P) are 6p $^2\Pi_{1/2}$, 6p $^2\Pi_{3/2}$, and 6p $^2\Sigma_{1/2}$. At long distances, spin-orbit becomes dominant and the eigenstates are characterized by the usual atomic case (c) notation $^{2S+1}L_J$.

D. DIM Hamiltonian

In order to study the potential energies and couplings in exciplexes with $n > 1$ helium atoms, we use an extended version of the diatomics in molecules (DIM) Hamiltonians used previously[44,48] for the valence electron of Ba$^+$. The total electronic Hamiltonian for Ba$^+$ interacting with n helium atoms is written as

$$H_{el}^n = H_{DIM} + H_{SO}, \qquad (9)$$

where H_{SO} is the spin-orbit Hamiltonian of Eq. (7) and H_{DIM} is a sum of electronic Hamiltonians for each pair of atoms,

$$H_{DIM} = \sum_{\alpha=1}^{n} H_{el}(\mathbf{R}_{Ba^+-\alpha}) - (n-1)H_{Ba^+}$$
$$+ \sum_{\alpha} \sum_{\alpha'>\alpha} \mathcal{V}_{He-He}(|\mathbf{R}_{\alpha'} - \mathbf{R}_{\alpha}|). \qquad (10)$$

In this equation, $\mathbf{R}_{Ba^+-\alpha} = \mathbf{R}_\alpha - \mathbf{R}_{Ba^+}$ is the distance vector from Ba^+ with vector position $\mathbf{R}_{Ba^+}$ to the αth He atom, with vector position $\mathbf{R}_\alpha$; $H_{el}(\mathbf{R}_{Ba^+-\alpha})$ is the electronic Hamiltonian of the Ba^+-αth He atom interaction; $\mathcal{V}_{He-He}$ is the He–He pair interaction taken from the literature;[49] and H_{Ba^+} is the isolated Ba^+ electronic Hamiltonian which is counted n times in the first term of the right-hand side of Eq. (10).

The overall matrix of H_{DIM} is expressed in the basis set of the effective Ba^+ orbitals $|k\rangle$ described in Secs. II B and II C. In order to do this, a common, space-fixed set of axes is chosen. The $\mathbf{W}$ matrix for each $H_{el}(\mathbf{R}_{Ba^+-\alpha})$ He_α–Ba^+ interaction was defined by Eq. (6) with the z axis parallel to the distance vector $\mathbf{R}_{Ba^+-\alpha}$. It is rotated to the common axes by a (block-diagonal) rotation matrix, with each block corresponding to the different L values. It is then extended to 18×18 by replicating the same matrix as a diagonal block for $M_S = -1/2$ and $1/2$. Finally H_{SO} is added and the total Hamiltonian is diagonalized. The same notation is used for the resulting eigenvectors as in the diatomic case [Eq. (8)], ψ_K, since they are also describing the electronic structure of Ba^+ and in the same basis set. Note that the coefficients $c_{K'K}$ depend on all the helium atom coordinates $\mathbf{R}_{Ba^+-\alpha}$. The eigenvectors are labeled in increasing energy order, with adiabatic following[50] in the case of a crossing.

III. METHODOLOGY FOR He···Ba⁺ PHOTODISSOCIATION STUDY

We use the potential energy curves and couplings presented in Sec. II B, to which spin-orbit interaction of Sec. II C is added, to investigate the photodissociation of the He···Ba⁺ complex from its ground 6s $^2S_{1/2}$ to its first excited electronic states 5d ^2D and 6p ^2P. The final state-resolved and total cross sections for photodissociation are determined using the energy-resolved (coupled-channel equations) approach.[51,52] This corresponds to photoexcitation spectra in which the bare ion is detected (total cross section), with the possibility of resolving its final electronic state (partial cross sections). All the final states energetically accessible in the spectral region of interest are considered: 6s $^2S_{1/2}$, 5d $^2D_{3/2}$ and 5d $^2D_{5/2}$, 6p $^2P_{1/2}$ and 6p $^2P_{3/2}$. The weak features appearing in the spectrum in addition to the strong (6p ^2P ← 6s ^2S) direct dissociation peaks are analyzed in terms of electronic predissociation of the He···Ba⁺ ion by comparing with quasibound state calculations. These resonances could play an important role in other dynamical processes involving the Ba^+ ion and a helium atom, like collisional relaxation of Ba^+ by a helium environment. In particular, experimental investigations on photoexcitation of helium nanodroplets doped with an alkali-like atom have shown that exciplexes are formed with the excited atom and one or a few helium attached to it.[17–19,23,30–32,53–56] The corresponding exciplex for Ba^+ would be characterized by one of the resonances identified in this work, hence its lifetime could be determined.

The main aspects of the method are summarized here for the sake of completeness. In the framework of the first order perturbation theory for electric dipole transitions, the partial cross section for photo-exciting the system is given by

$$\sigma_{jE\leftarrow i}(h\nu) \propto \left|\langle \Psi_{jE}|\vec{\mu}\cdot\vec{\mathcal{E}}|\Psi_i\rangle\right|^2, \qquad (11)$$

where Ψ_i is the initial (bound) wave function of He···Ba⁺ in its ground electronic state with energy E_i and Ψ_{jE} is the final continuum wave function for He + Ba⁺ (j) in the electronic state j of the ion, with energy E; $\vec{\mathcal{E}}$ is the photon polarization and $h\nu$ its energy ($h\nu = E - E_i$); and $\vec{\mu}$ is the transition dipole moment.

The bound state wave function for the ground electronic state and for the quasibound states used in the discussion of the results is obtained by finite difference followed by Numerov-Cooley integration[57,58] from 1.8 up to 80 Å with interval 0.05 Å for the adiabatic electronic state of interest. The continuum wave function is expanded in the case (a) or case (c) electronic basis set using the diabatized Hamiltonian and integrated from 1.5 to 200 Å in steps of 0.002 Å using the De Vogelaere algorithm.[59,60]

Finally, the total cross section $\sigma_{E\leftarrow i}(h\nu)$ for dissociative photoionization of He···Ba⁺ at energy $E = E_i + h\nu$ and the final state distributions $P_j(h\nu)$ of the Ba^+ fragments are given by

$$\sigma_{E\leftarrow i}(h\nu) = \sum_j \sigma_{jE\leftarrow i}(h\nu), \qquad (12)$$

$$P_j(h\nu) = \frac{\sigma_{jE\leftarrow i}(h\nu)}{\sigma_{E\leftarrow i}(h\nu)}. \qquad (13)$$

The transition dipole moment $\vec{\mu}$ in Eq. (11) is taken as the one of Ba^+. Since the ground electronic state of Ba^+ in the complex has small 6p ^2P and 5d ^2D components, both the 6p ^2P ← 6s ^2S and 5d ^2D ← 6p ^2P transition dipole moments are needed, the 5d ^2D ← 6s ^2S one being zero because it corresponds to a forbidden transition. We have estimated the ratio of these dipole moments from the ratio of the sum of the corresponding transition intensities of Ba^+ taken from Ref. 47. The calculations were performed for the most abundant isotope of barium, ^{138}Ba ($M = 137.905\,247\,2(5)u$[61]).

IV. RESULTS: PHOTO-DISSOCIATION SPECTRA

There are three bound states for He···Ba⁺ in its ground electronic state with the potential used. The ground state $v = 0$ is at $E_0 = -12.704$ cm^{-1} from the dissociation threshold. This is the only level populated at the droplet temperature of 0.4 K and consequently, it is the one used in the calculations for the He···Ba⁺ photodissociation spectrum.

A. Total photodissociation spectra

The calculated photodissociation cross section for He···Ba⁺ in the vicinity of the 6p ^2P ← 6s ^2S transition is shown in Fig. 3. As expected from the adiabatic potential energy curves of He···Ba⁺ shown as the top plot in Fig. 4, the 6p ^2P ← 6s ^2S photodissociation spectrum is dominated
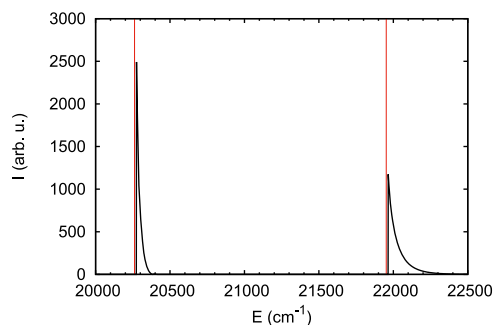
FIG. 3. Oscillator strength for the photo-dissociation spectrum of He$\cdots$Ba$^+$ in the vicinity of the Ba$^+$ 6p ^{2}P$_{1/2}$ ← 6s ^{2}S$_{1/2}$ and 6p ^{2}P$_{3/2}$ ← 6s ^{2}S$_{1/2}$ transitions. The vertical red lines show the atomic ion excitations: 20 261 cm^{-1} for Ba$^+$ 6p ^{2}P$_{1/2}$ and 21 952 cm^{-1} for Ba$^+$ 6p ^{2}P$_{3/2}$.[62,63] The intensity scale is in arbitrary units.

by direct photodissociation to the He + Ba$^+$ continuum: one lower energy peak corresponding to $^2\Pi_{1/2}$ excitation of the dimer which leads to He + Ba$^+$ 6p ^{2}P$_{1/2}$ and one higher energy peak corresponding to $^2\Pi_{3/2}$ and $^2\Sigma_{1/2}$ excitation which leads to He + Ba$^+$ 6p ^{2}P$_{3/2}$ (the Franck-Condon region extends roughly between 4 and 7 Å; see the wave function in Fig. 2 or in the top plot of Fig. 4).

There is also a weak spectrum in the vicinity of the 5d ^{2}D ← 6s ^{2}S transition. It appears because of intensity borrowing
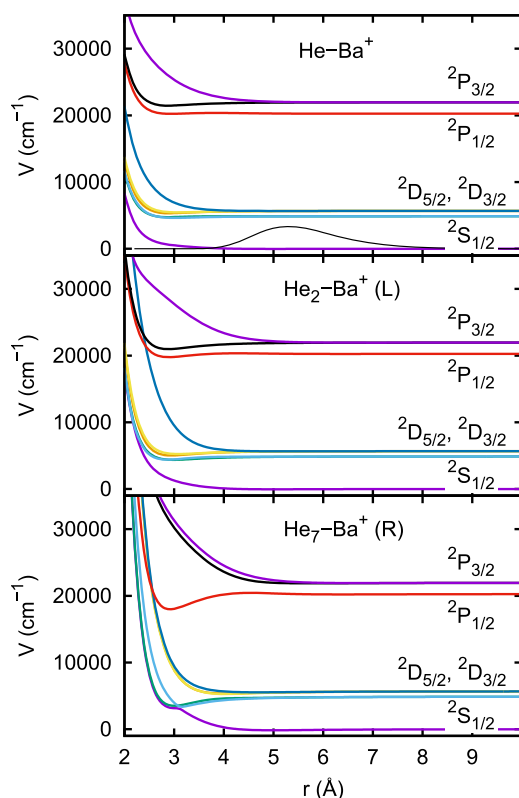
FIG. 4. Potential energy curves for He$\cdots$Ba$^+$ (top plot); linear He–Ba$^+$–He (middle plot); ring-shaped He$_7$Ba$^+$ (bottom plot). In the case of the linear He–Ba$^+$–He excimer, the r coordinate is the symmetric elongation of the HeBa$^+$ distance. In the case of the ring-shaped He$_7$Ba$^+$ excimer, the seven helium atoms are set equidistant on a ring of radius r around Ba$^+$. The bound state wave function of He$\cdots$Ba$^+$ is also represented in the top plot in order to visualize the Franck-Condon region.

from electronic state mixing by the helium atom. It is shown in the supplementary material.

B. Lifetime of the He$\cdots$Ba$^+$ exciplex

Both the 6p $^2\Pi_{1/2}$ and 6p $^2\Pi_{3/2}$ potential energy curves contain several vibrational levels. They are called quasibound states in the following since they can in principle decay to the ground or one of the 5d ^{2}D states because of helium induced electronic couplings. Their lifetime depends on the existence and intensity of these couplings. In the photodissociation spectra, they appear as resonances (corresponding to Feshbach resonances in He–Ba$^+$ collisions) with a linewidth inversely proportional to their lifetime. Their intensity depends also on Franck-Condon factors with the ground state, but their central energy and linewidth are intrinsic properties that are accurately determined in our calculations. Even if they do not show in the photodissociation spectrum because of their weak intensities, they may be involved in collisional relaxation or other processes.

These resonances are analyzed in the supplementary material and show good agreement when compared with bound state energies calculated by Moroshkin and Kono.[38] All their widths were found to be smaller than 10^{-10} cm^{-1}, which implies lifetimes longer than 50 ms. This is much longer than the Ba$^+$ 6p ^{2}P fluorescence lifetime[64] of 6.32 ns (6p ^{2}P$_{3/2}$) or 7.92 ns (6p ^{2}P$_{1/2}$). Hence if a He$\cdots$Ba$^+$ excimer is formed in the course of the dynamics, it is likely to fluoresce before relaxing to a lower electronic state by helium-induced transition.

Similar resonances are observed when exciting in the region of the 5d ^{2}D states; see the supplementary material.

V. HELIUM-INDUCED ELECTRONIC COUPLINGS IN He$_n$Ba$^+$ EXCIPLEXES

As explained in the Introduction, helium-induced electronic relaxation has been invoked several times in the context of excimers in superfluid bulk helium and helium nanodroplets. These excimers are generally located inside a "bubble" and have He–Ba$^+$ distances of ~3.2 Å, i.e., shorter than the distance between Ba$^+$ and the helium atoms forming the "bubble" around the ion (see Sec. V C). Hence they are good candidates to explore the possibility for helium-induced electronic transitions because the corresponding couplings are usually stronger at short distances.

In this section, we study the potential energy curves and electronic mixing coefficients for two structures that can lead to excimers,[39,45] i.e., linear He$_2$Ba$^+$ and ring-shaped He$_7$Ba$^+$, in order to explore the possibility for helium-induced electronic transitions.

A. He$_n$Ba$^+$ exciplexes' potential energy curves

Figure 4 displays the potential energy curves for He$\cdots$Ba$^+$ (top), linear He–Ba$^+$–He (middle), and ring-shaped He$_7$Ba$^+$ exciplexes (bottom). These potential energy curves are obtained by diagonalizing the DIM+SO Hamiltonian obtained as described in Refs. 39 and 44, except that here the DIM Hamiltonian includes S-P-D couplings as described in

Sec. II D. On the scale of the drawing, they are the same as the ones obtained without these couplings.[50] This is not surprising since they were obtained from the same *ab initio* curves.

The He···Ba$^+$ complex has a deep minimum of 486 cm^{-1} at 2.885 Å in the 6p $^2\Pi_{3/2}$ curve, corresponding to excimer formation with no barrier. The other two 6p ^{2}P states exhibit a flat van der Waals well at long distances (~7 Å) with the rest of the 6p $^2\Sigma_{1/2}$ curve repulsive and the 6p $^2\Pi_{1/2}$ curve exhibiting a small well at ~3 Å, separated from the van der Waals well by a barrier.

The linear He–Ba$^+$–He configuration has similar potential energy curves, with deeper wells in the 6p $^2\Pi_{3/2}$ and 6p $^2\Pi_{1/2}$ curves. Note that the highest 5d ^{2}D curve crosses all the 6p ^{2}P curves at short distances.

The ring $n = 7$ configuration has a deep well in the lowest p curve. Caution should be taken in labeling the curves in this case. The natural quantization axis, taken as the z axis, is the one perpendicular to the plane of the helium atoms (C_7 symmetry axis). In the case of the $n = 1$ or 2 complexes, the quantization z axis was running from Ba$^+$ to one of the helium atoms. Hence a Σ curve is repulsive for $n = 1$ or 2 (apart from the long distance van der Waals well), whereas it is attractive and carries the deep exciplex well at short distances for the $n = 7$ ring structure. This is not merely a question of notation since as explained in Sec. V B it leads to an avoided crossing which can be responsible for fine structure relaxation.

B. Ba$^+$ fine structure relaxation in the ring exciplex

In this section, we show that He$_n$–Ba$^+$ interaction in a ring configuration can induce fine structure relaxation of Ba$^+$ 6p ^{2}P$_{3/2}$.

The 6p ^{2}P potential energy curves of the $n = 7$ ring isomer are shown in more detail in Fig. 5. There are several interesting points to note. First, all the P energy curves have a long range van der Waals well. The one having the best overlap with the ground electronic state is the lowest of the two curves leading to Ba$^+$ 6p ^{2}P$_{3/2}$, but all three have a non-negligible possibility for direct bound-bound excitation. Second, the curve leading to 6p ^{2}P$_{1/2}$ exhibits a barrier between the region accessed by Franck-Condon excitation and the deep excimer well. Hence upon 6p ^{2}P$_{1/2}$ excitation the well can only be accessed from the tail of the ground bound state wave function or by tunneling. Third, it is surprising at first glance that the deep excimer potential well should be carried by the lowest curve of the p states. It is due to the avoided crossing introduced in Sec. V A and similar to the one noted by Moroshkin *et al.*[9] for alkalis in solid helium. It is visualized by plotting the diagonal matrix elements of the total Hamiltonian in the asymptotic (i.e., atomic) basis set as dashed lines in Fig. 5. The change in character of the corresponding electronic states is evidenced in the top plot of that figure. At long distances where spin-orbit interaction is dominant, the eigenstates are the spin-orbit eigenstates of the isolated Ba$^+$. Hence the lowest one is 6p ^{2}P$_{1/2}$ Kramer's pair of levels which is a linear combination of 2/3 of p$_{\pm1}$ and 1/3 of p$_0$ and the next higher one is the 6p ^{2}P$_{3/2}$ pair with |Ω| = 1/2, which is a linear combination of 2/3 of p$_0$ with 1/3 of p$_{\pm1}$. The other 6p
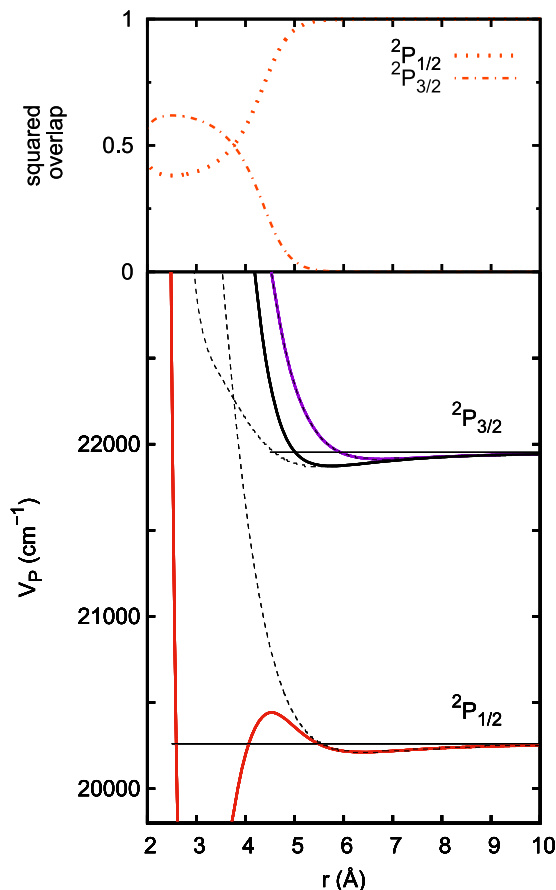
FIG. 5. Top: Squared overlap $|\langle\psi_{K'}(r_\infty)|\psi_K(r)\rangle|^2$ of the lowest P energy eigenstate $\psi_K(r)$, $K = 13$, with the asymptotic 6p ^{2}P$_{1/2}$ ($\psi_{K'}(r_\infty)$, $K' = 13$) and 6p ^{2}P$_{3/2}$, |Ω| = 1/2 ($\psi_{K'}(r_\infty)$, $K' = 15$) states for the ring-shaped He$_7$Ba$^+$ excimer. $\psi_{K'}(r)$ are the electronic eigenvectors defined at the end of Sec. II D, and r_∞ is taken as 10 Å. Bottom: Focus on the P potential energy curves of the ring-shaped He$_7$Ba$^+$ complex as a function of the He–Ba$^+$ distance. The dotted lines are the diagonal matrix elements of the total Hamiltonian in the asymptotic (i.e., atomic) basis set, in order to visualize the avoided crossing. Note that the one corresponding to the 6p ^{2}P$_{3/2}$ state with |Ω| = 3/2 is superimposed with the highest energy curve.

^{2}P$_{3/2}$ pair corresponds to |Ω| = 3/2 and is purely p$_{\pm1}$. At short distances where the difference between Π and Σ interactions is larger than the spin-orbit splitting, the eigenstates are close to the ones of the H_{DIM} electrostatic Hamiltonian. The lowest ones in energy are the p$_z$ (p$_0$) state pair which are strongly attractive, all the He atoms being in the nodal plane. Both p$_{\pm1}$ (or p$_x$, p$_y$) orbitals give a repulsive curve since they both lie in the molecular plane. Hence the character of the lowest p curve changes from the asymptotic region where it is 2/3 Π in the He$_7$Ba$^+$ axes to the inner well region where it is mostly Σ. It corresponds to an avoided crossing between the Σ curve exhibiting the deep well at short distances and going asymptotically to 6p ^{2}P$_{3/2}$ and the Π curve going asymptotically to 6p ^{2}P$_{1/2}$. This is illustrated in the upper plot of Fig. 5, which shows the overlap of the lowest P eigenstate with the eigenstates in the asymptotic region ($R = 10$ Å). The two states exchange at $R \simeq 3.75$ Å. The mixing starts being visible around 5 Å, which is the minimum of the well in the ground electronic state. As a result, the curve leading to exciplex formation exhibits a maximum at 4.55 Å, which represents a barrier of 180 cm^{-1} above the asymptotic energy. The exciplex well at 2.9 Å is 2271 cm^{-1}

deep, whereas the van der Waals well at 6.4 Å is of 49.8 cm^{-1}. By contrast, the other two higher curves only have a van der Waals well.

Hence it can be expected that upon excitation to the lower 6p $^2P_{3/2}$ curve there will be a transition to the curve corresponding to the 6p $^2P_{1/2}$ asymptotic state, leading to excimer formation and resulting in fine structure relaxation. The importance of this mechanism will have to be confirmed by a dynamics study. It could be quite frequent since the bubble configuration in the ground electronic state can provide ring configurations for almost any orientation of the excitation.

C. Ba$^+$ fine structure relaxation in the linear *n* = 2 exciplex

Many possible couplings between electronic states are forbidden by the high symmetry of the exciplexes. However, these exciplexes are formed at rather long distances since the Franck-Condon region for their excitation corresponds to the bubble state of the ground electronic level. As shown by Fiedler *et al.*,[65] Leal *et al.*,[66] and more recently by Batulin *et al.*,[67] the bubble radius is about 4.5 Å, and DFT calculations[44,65,66] show that it is surrounded by a high density shell structure. This would locate the Franck-Condon region for Ba$^+$ in liquid helium at about the same He–Ba$^+$ distance as for the He···Ba$^+$ dimer, 4 to 8 Å with a maximum at ∼5.2 Å, as materialized by the wave function in Figs. 2 and 4. The energies corresponding to these excited configurations are substantially larger than the well minima at shorter distances. Hence the exciplexes are formed with a lot of initial internal, i.e., vibrational, energy. Many of the excited vibrational modes can break the cylindrical symmetry of the system. We show here as an example how the bending mode of the *n* = 2 excimer can induce fine structure relaxation.

The minimum energy structure of the *n* = 2 excimer is linear. Assuming that it is created from the spherical bubble of the ground electronic state, it is expected that the internal energy will be distributed among the stretching modes and the bending mode. The bending mode breaks cylindrical symmetry and hence makes it possible to mix the 6p $^2\Pi_{3/2}$ state with the 6p $^2\Pi_{1/2}$ state.

This is illustrated in Fig. 6, which shows the eigenenergies and the squared overlaps of the *p* eigenvectors with the ones at the linear configuration, as a function of the bending angle ϕ_b (He–Ba$^+$–He). The He–Ba$^+$ distance is taken as that of the minimum energy configuration of the 6p $^2\Pi_{3/2}$ state, 2.88 Å. At the minimum energy configuration ($\phi_b = \pi$), the top three eigenstates labeled in increasing energy order as P$_1$, P$_2$, and P$_3$, are mostly 6p $^2\Pi_{1/2}$, 6p $^2\Pi_{3/2}$, and 6p $^2\Sigma_{1/2}$, respectively, with the exciplex corresponding to the $\Pi_{3/2}$ curve. For a pure p state in the linear configuration, the $\Pi_{3/2}$ eigenvector cannot mix with the other two since it is both an eigenstate of the electronic Hamiltonian ($\Lambda = \pm 1$) and of the spin-orbit Hamiltonian ($\Omega = \pm 3/2$). This situation changes when the exciplex is no longer linear. With the amount of internal energy of the order of the 6p $^2\Pi_{3/2}$ excimer well depth, 980 cm^{-1}, the bending angle can deviate from π down to 2.5 rad. What is very interesting is that the lowest two eigenstates start mixing as
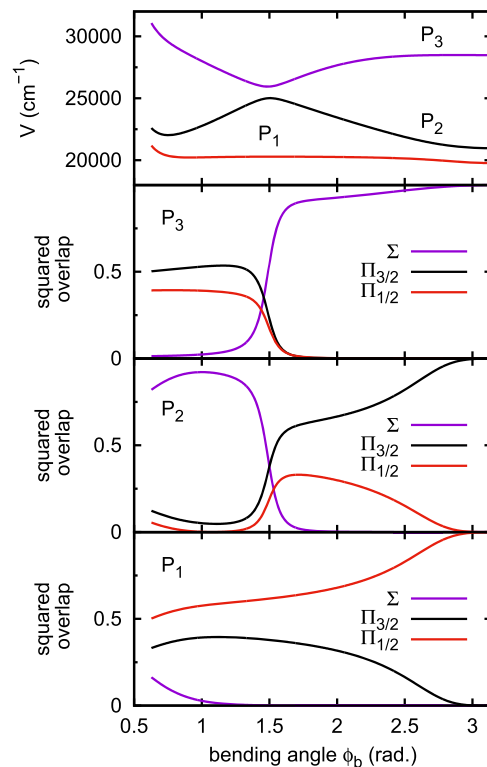
FIG. 6. Top plot: Potential energy curves of the P states of He$_2$Ba$^+$ [ψ_K defined at the end of Sec. II D, labeled P$_1$ ($K = 13$), P$_2$ ($K = 15$), P$_3$ ($K = 17$) in increasing energy order] as a function of the bending (He–Ba$^+$–He) angle ϕ_b for r = 2.88 Å (equilibrium distance in the exciplex). Lower three plots: Squared overlap $|\langle \psi_{K'}(\pi)|\psi_K(\phi_b)\rangle|^2$ of the He$_2$Ba$^+$ P$_3$ ($K = 17$, top plot), P$_2$ ($K = 15$, middle plot), P$_1$ ($K = 13$, bottom plot), with the Σ ($\psi_{17}(\pi)$), $\Pi_{3/2}$ ($\psi_{15}(\pi)$), and $\Pi_{1/2}$ ($\psi_{13}(\pi)$) eigenvectors of the linear configuration as a function of ϕ_b for $r = 2.88$ Å.

soon as it deviates from π, whereas the highest energy state remains mostly Σ in character up to $\phi_b = \pi/2$. Hence excitation of the bending vibration, or even the zero-point amplitude of the bending angle, can induce fine structure relaxation from 6p $^2\Pi_{3/2}$ to 6p $^2\Pi_{1/2}$.

D. Electronic couplings between different Ba$^+$ states in exciplexes

In this section, we analyze the mixing of the P, D, and S states of Ba$^+$ induced by the helium atoms in different configurations, in order to identify possible pathways for non-radiative relaxation of Ba$^+$ 6p $^2P_{3/2}$ or 6p $^2P_{1/2}$ to the lower electronic states (5d ^2D or 6s ^2S). The eigenstates of Ba$^+$ in interaction with helium are labeled as explained at the end of Sec. II D. They are denoted as $\widetilde{S}$, $\widetilde{P}$, and $\widetilde{D}$ to differentiate them from the S, P, and D states of the isolated Ba$^+$.

The potential energy curves of He$_n$Ba$^+$ in the $n = 2$ linear and $n = 7$ ring configurations already presented in Fig. 4 are completed by the mixing coefficients presented in Fig. 7. These coefficients characterize the contribution of the bare Ba$^+$ 6s ^2S, 5d ^2D, and 6p ^2P states to the corresponding states of the exciplexes. They are defined as follows:

$$C_{\widetilde{L},L'} = \sum_K \sum_{K'} |c_{K'K}|^2, \qquad (14)$$

where $c_{K'K}$ are the coefficients of eigenstate K in the basis functions $|\psi_{K'}\rangle$ as introduced at the end of Sec. II D. K runs
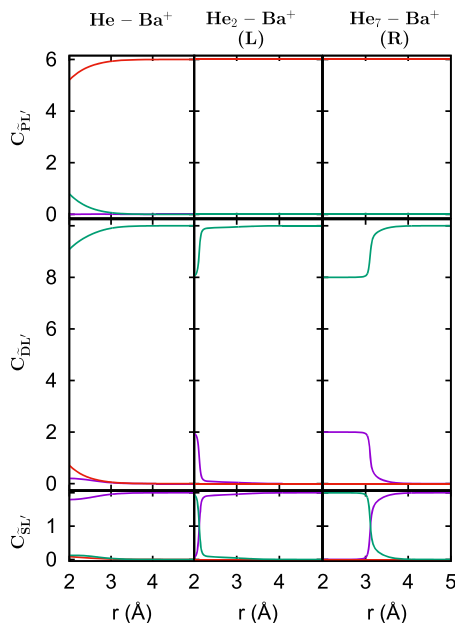
FIG. 7. Mixing coefficients for He$\cdots$Ba$^+$, linear He$_2$Ba$^+$, and ring-shaped He$_7$Ba$^+$. The bottom, middle, and top plots give the decomposition of the adiabatic ground $6\widetilde{S}$ and excited $5\widetilde{D}$ and $6\widetilde{P}$ states, into Ba$^+$ electronic states 6S (purple curves), 5D (green curves), and 6P (red curves), respectively [$C_{\widetilde{S}L'}$, $C_{\widetilde{D}L'}$, and $C_{\widetilde{P}L'}$ defined in Eq. (14)]. Given the degeneracy of the S, D, and P states, the asymptotic value of $C_{\widetilde{S}S}$, $C_{\widetilde{D}D}$, and $C_{\widetilde{P}P}$ is 2, 10, and 6, respectively.

over all the eigenstates $|\psi_K\rangle$ corresponding to $\widetilde{L}$ (i.e., $\widetilde{S}$, $\widetilde{P}$, or $\widetilde{D}$) and K' runs over the basis functions corresponding to state L' of Ba$^+$ (S, P, or D).

Helium-induced electronic transitions should occur in regions where potential energy curves are close to each other, usually in the repulsive part or in the so-called avoided crossings. Note that the $n = 2$ and $n = 7$ excimers have an additional plane of symmetry containing the barium ion so that curves belonging to different symmetry classes of their symmetry point group ($D_{\infty h}$ for $n = 2$, D_{7h} for $n = 7$) can cross without mixing. This is the case for curves originating from p orbitals, which have no common irreducible representation with the s or d orbitals.[68] Hence in Fig. 4 the crossing of the highest $\widetilde{D}$ state with the $\widetilde{P}$ ones for $n = 2$ and of the three higher of $\widetilde{D}$ states with the lower $\widetilde{P}$ one for $n = 7$ are "real crossings" and do not induce electronic relaxation.

In the case of the $n = 1$ excimer, there is no obvious avoided crossing in Fig. 4. However, examination of the mixing coefficients in the left column of Fig. 7 reveals some mixing of the states in the $2.0 \leq r \leq 3.2$ Å range. The minimum of the $\widetilde{P}$ wells is at 2.94 Å (-30.3 cm^{-1}) for the lowest and 2.88 Å (-485.9 cm^{-1}) for the intermediate state (the highest one only has a van der Waals well). Hence if the He$\cdots$Ba$^+$ $6\widetilde{P}$ exciplex is formed in the course of the photodissociation, there is a small probability that it will dissociate to the lower $5\widetilde{D}$ and $6\widetilde{S}$ states. As concluded above in the study of the resonances in the photodissociation spectrum of He$\cdots$Ba$^+$, the bound states in the 6p $^2P_{3/2}$ well are therefore predissociated, but their lifetime is quite long.

The linear $n = 2$ excimer potential energy curves reveal several interesting features. First, the highest $\widetilde{D}$ curve intersects all three $\widetilde{P}$ curves and notably the two lower ones which

are mostly Π in the region of their well. However, because of symmetry reasons evoked earlier, this cannot result in predissociation of the $\widetilde{P}$ states. Hence the $\widetilde{P}$ states remain 100% P, as evidenced from the $C_{\widetilde{P},P}$ coefficient which remains equal to six for all distances. This situation can change if symmetry is broken; see Sec. V E.

Another interesting feature is the avoided crossing between the $6\widetilde{S}$ and the lower $5\widetilde{D}$ curves in the vicinity of $r = 2.12$ Å. It is clearly seen in the decomposition of the $6\widetilde{S}$ He$_2$Ba$^+$ states in Fig. 7, which switches from 6S at long distances to 5D for $r = 2$ Å. Since this is in the repulsive region for both curves, it could only become important in the case of dissociative dynamics occurring at energies close to that of the avoided crossing, $V = 11\,900$ cm^{-1}. This is possible if the exciplex was initially created in one of the $6\widetilde{P}$ states which could then be predissociated to the highest $\widetilde{D}$ state in an inhomogeneous environment (to break cylindrical symmetry).

Helium induced transitions are also encountered in the case of the $n = 7$ ring isomer. In this case only the lowest $6\widetilde{P}$ state has a well, but it is deeper: 2272 cm^{-1} at $r = 2.9$ Å. It is intersected by the three highest $5\widetilde{D}$ curves going asymptotically to the 5d $^2D_{5/2}$ level. For the same symmetry reason as in the linear $n = 2$ excimer, this does not induce transition unless symmetry is broken by the environment. In addition, there is also an avoided crossing. As can be seen by looking at the $6\widetilde{S}$ He$_7$Ba$^+$ states in Fig. 7, they switch from 6S at long distances to 5D at shorter distances, and this crossing occurs at longer distances than for He$_2$Ba$^+$: ~3 Å, which makes the 5d $^2D \rightarrow$ 6s ^2S relaxation even more probable in the exciplex configuration where He–Ba$^+$ distances are ~2.9 Å.

E. Influence of exciplex vibrations on electronic couplings

As concluded in Sec. V D, many possible couplings between electronic states are forbidden by the high symmetry of the exciplexes. In the case of the linear $n = 2$ excimer, for instance, the two $6\widetilde{P}$ states are mostly $|\Lambda| = 1$, while the highest $5\widetilde{D}$ state is mostly $\Lambda = 0$, hence the system has to get out of cylindrical symmetry for the P-D coupling to become efficient. This could occur if the helium environment becomes inhomogeneous and/or upon excitation of a non-symmetric vibration. As an example, Fig. 8 shows the S-P-D electronic state coefficients C_L as a function of the bending angle ($\phi_b = \pi$ at equilibrium) for selected eigenstates which exhibit some degree of mixing. The C_L are defined as

$$C_L = \sum_K \sum_{K'} |c_{K'K}|^2, \qquad (15)$$

where $c_{K'K}$ was introduced at the end of Sec. II D, K runs over Kramer's pair of the Kramer's pair of eigenvectors, and K' runs over the basis functions corresponding to state L of Ba$^+$ (S, P, or D). Both the highest state, corresponding to 6p $^2\Sigma_{1/2}$ at the linear configuration, and the intermediate state, corresponding to 6p $^2\Pi_{3/2}$, start showing some mixing with D states as soon as the bending angle gets away from the linear configuration. The effect is even larger at shorter distances (not shown here), which can be accessed in the case where the excimer is formed with a lot of internal energy. In this case, even the lower P state shows some mixing with the D states.
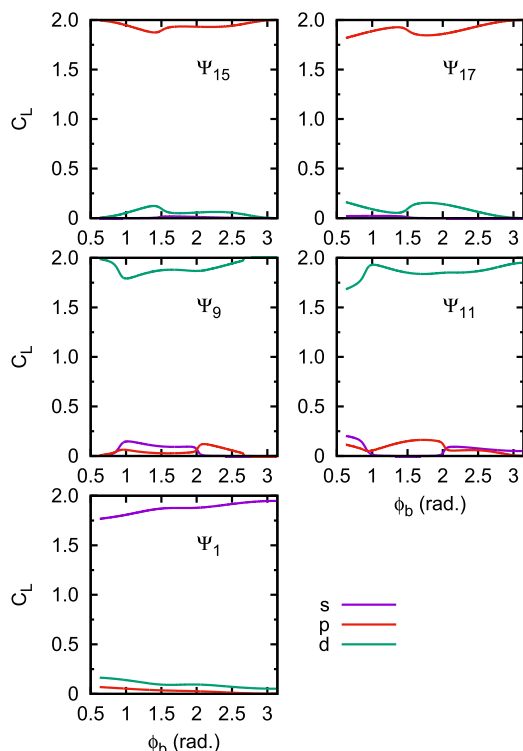
FIG. 8. Electronic state coefficients C_L [defined in Eq. (15)] as a function of the bending (He–Ba$^+$–He) angle ϕ_b at $r = 2.88$ Å for selected He$_2$Ba$^+$ eigenstates ψ_K (in parentheses their assignment at $\phi_b = \pi$): $K = 1$ (6s $^2\Sigma_{1/2}$); 9 (5d $^2\Delta_{5/2}$); 11 (5d $^2\Sigma_{1/2}$); 15 (6p $^2\Pi_{3/2}$); and 17 (6p $^2\Sigma_{1/2}$) in increasing energy order. If the state is "pure," like most of them at $\phi_b = \pi$, the result is 2 for the corresponding L and 0 for the others.

These shorter distances, at which interelectronic state couplings are stronger and can induce predissociation, can be accessed in the course of the dynamics following Ba$^+$ 6p ^{2}P photoexcitation. As already mentioned, exciplexes are initially formed with a lot of internal energy. In addition, if fine structure relaxation occurs, additional energy is brought into the system. For instance, if it occurred at the minimum energy distance of the 6p $^2\Pi_{3/2}$ curve of the $n = 2$ excimer, this would correspond to 1200 cm^{-1} of additional energy. With this amount of kinetic energy, the classical turning point in the $\Pi_{1/2}$ state is 2.475 Å. At this distance, the couplings between different electronic states of Ba$^+$ are much stronger. In a complex already distorted because of the amount of internal energy with which it was initially formed, this could lead radiationless transitions from 6p ^{2}P to 5d ^{2}D and then 5d ^{2}D to 6s ^{2}S.

VI. SUMMARY AND OUTLOOK

We have designed a model for the He$_n$–Ba$^+$ electronic Hamiltonian in order to explore the possibility for helium-induced electronic transitions of Ba$^+$ excited to a 6p ^{2}P state. Application of this Hamiltonian to the calculation of the photodissociation of He$\cdots$Ba$^+$ gives excited bound state lifetimes exceeding by far the radiative lifetime. However, using this Hamiltonian in configurations of Ba$^+$ with more than one He has revealed the possibility for helium induced transitions even in symmetric environments, like the fine structure relaxation in the $n = 7$ ring configuration. In addition we have

shown that bending vibrations can induce fine structure or other electronic relaxation ("internal conversion") by breaking cylindrical symmetry. We believe that the large amount of kinetic energy released in these processes could be partly transferred to the impurity, which could explain the ejection of Ba$^+$ or excimers from the droplet.

These mechanisms for fine structure relaxation and inter-electronic state relaxation are shown here for Ba$^+$, but the model could in principle be applied to any one-electron system such as other alkali-earth ions and alkali atoms in solid or liquid helium and in droplets. For instance, electronic relaxation was reported for cesium in solid helium.[9] Note that even in cold ($T = 1.35$ to 30 K) helium gas where density is low, fine structure relaxation has been observed and attributed to collisional relaxation of the He$\cdots$Ba$^+$ exciplex.[36–38] In helium droplets, the other alkali-earth ions should exhibit electronic relaxation processes similar to those presented here for Ba$^+$.

In the case of neutral alkali (Ak) atoms, there is an important difference due to their localization at the surface of the droplet, which makes the formation of a linear or ring excimer or even bubble configuration unlikely. As shown in He-DFT and He-TDDFT simulations, only one of the two minima of the potential well of the np $^2\Pi_{3/2}$ state, the one closer to the droplet surface, is populated, the other one being on the other side of the alkali with respect to the droplet. Thus only the 1-atom HeAk np $^2\Pi_{3/2}$ excimer can be formed.[12] This is in full agreement with quantum Monte Carlo calculations carried out for Rb atoms.[69] Hence if electronic relaxation due to helium occurs in these excited atoms, it could only be due to the non-symmetric helium environment.

Very recently, a combined experimental and theoretical study has shown that spin-orbit relaxation is indeed important for alkalis on ^{4}He droplets.[70] The experiment showed that $^2\Pi_{3/2}$ excitation of a Rb atom bound to a droplet leads to the formation of a stable RbHe exciplex which detaches from the droplet. The accompanying theoretical He-TDDFT study also showed the formation of an exciplex, but only by invoking $^2\Pi_{3/2} \rightarrow {}^2\Pi_{1/2}$ relaxation could detachment be explained.

The electronic Hamiltonian model presented in this work provides a tool for studying electronic relaxation in a wide range of helium environments. The couplings responsible for fine structure and inter-electronic state relaxation need to be confirmed by a dynamics study, which is currently under way in our laboratories.

SUPPLEMENTARY MATERIAL

See supplementary material for the 5d ^{2}D ← 6s ^{2}S photodissociation spectrum which is induced by electronic mixing in He$\cdots$Ba$^+$, as well as details on the 6p ^{2}P ← 6s ^{2}S and 5d ^{2}D ← 6s ^{2}S spectra: final state resolved cross sections and resonance energies compared to quasibound state energies.

ACKNOWLEDGMENTS

[1] K. B. Whaley, Int. Rev. Phys. Chem. **13**, 41 (1994).
[2] J. P. Toennies and A. F. Vilesov, Annu. Rev. Phys. Chem. **49**, 1 (1998).
[3] F. Stienkemeier and A. F. Vilesov, J. Chem. Phys. **115**, 10119 (2001).
[4] J. P. Toennies and A. F. Vilesov, Angew. Chem., Int. Ed. **43**, 2622 (2004).
[5] M. Y. Choi, G. E. Douberly, T. M. Falconer, W. K. Lewis, C. M. Lindsay, J. M. Merritt, P. L. Stiles, and R. E. Miller, Int. Rev. Phys. Chem. **25**, 15 (2006).
[6] M. Barranco, R. Guardiola, E. S. Hernández, R. Mayol, J. Navarro, and M. Pi, J. Low Temp. Phys. **142**, 1 (2006).
[7] F. Stienkemeier and K. K. Lehmann, J. Phys. B: At., Mol. Opt. Phys. **39**, R127 (2006).
[8] J. Tiggesbäumker and F. Stienkemeier, Phys. Chem. Chem. Phys. **9**, 4748 (2007).
[9] P. Moroshkin, A. Hofer, and A. Weis, Phys. Rep. **469**, 1 (2008).
[10] K. Szalewicz, Int. Rev. Phys. Chem. **27**, 273 (2008).
[11] M. Mudrich and F. Stienkemeier, Int. Rev. Phys. Chem. **33**, 301 (2014).
[12] F. Ancilotto, M. Barranco, F. Coppens, J. Eloranta, N. Halberstadt, A. Hernando, D. Mateo, and M. Pi, Int. Rev. Phys. Chem. **36**, 621 (2017).
[13] J. Dupont-Roc, Z. Phys. B **98**, 383 (1995).
[14] S. Kanorsky, A. Weis, M. Arndt, R. Dziewior, and T. Hänsch, Z. Phys. B **98**, 371 (1995).
[15] T. Kinoshita, K. Fukuda, and T. Yabuzaki, Phys. Rev. B **54**, 6600 (1996).
[16] F. Stienkemeier, J. Higgins, C. Callegari, S. I. Kanorsky, W. E. Ernst, and G. Scoles, Z. Phys. D **38**, 253 (1996).
[17] J. Reho, C. Callegari, J. Higgins, W. E. Ernst, K. K. Lehmann, and G. Scoles, Faraday Discuss. **108**, 161 (1997).
[18] J. Reho, J. Higgins, C. Callegari, K. K. Lehmann, and G. Scoles, J. Chem. Phys. **113**, 9686 (2000).
[19] J. Reho, J. Higgins, K. K. Lehmann, and G. Scoles, J. Chem. Phys. **113**, 9694 (2000).
[20] M. Theisen, F. Lackner, and W. E. Ernst, Phys. Chem. Chem. Phys. **12**, 14861 (2010).
[21] F. Lackner, G. Krois, M. Theisen, M. Koch, and W. E. Ernst, Phys. Chem. Chem. Phys. **13**, 18781 (2011).
[22] E. Loginov and M. Drabbels, Phys. Rev. Lett. **106**, 083401 (2011).
[23] E. Loginov, C. Callegari, F. Ancilotto, and M. Drabbels, J. Phys. Chem. A **115**, 6779 (2011).
[24] M. Theisen, F. Lackner, and W. E. Ernst, J. Chem. Phys. **135**, 074306 (2011).
[25] A. Hernando, M. Barranco, M. Pi, E. Loginov, M. Langlet, and M. Drabbels, Phys. Chem. Chem. Phys. **14**, 3996 (2012).
[26] F. Lackner, G. Krois, M. Koch, and W. E. Ernst, J. Phys. Chem. Lett. **3**, 1404 (2012).
[27] N. B. Brauer *et al.*, Phys. Rev. Lett. **111**, 153002 (2013).
[28] F. Lackner, G. Krois, and W. E. Ernst, Mol. Phys. **111**, 2118 (2013).
[29] E. Loginov, A. Hernando, J. A. Beswick, N. Halberstadt, and M. Drabbels, J. Phys. Chem. A **119**, 6033 (2015).
[30] G. Droppelmann, O. Bünermann, C. P. Schulz, and F. Stienkemeier, Phys. Rev. Lett. **93**, 023402 (2004).
[31] C. P. Schulz, P. Claas, and F. Stienkemeier, Phys. Rev. Lett. **87**, 153401 (2001).
[32] C. Giese, T. Mullins, B. Grüner, M. Weidemüller, F. Stienkemeier, and M. Mudrich, J. Chem. Phys. **137**, 244307 (2012).
[33] J. von Vangerow, O. John, F. Stienkemeier, and M. Mudrich, J. Chem. Phys. **143**, 034302 (2015).
[34] J. von Vangerow, F. Coppens, A. Leal, M. Pi, M. Barranco, N. Halberstadt, F. Stienkemeier, and M. Mudrich, J. Phys. Chem. Lett. **8**, 307 (2017).
[35] H. J. Reyher, H. Bauer, C. Huber, R. Mayer, A. Schafer, and A. Winnacker, Phys. Lett. A **115**, 238 (1986).
[36] Y. Fukuyama, Y. Moriwaki, and Y. Matsuo, Phys. Rev. A **69**, 042505 (2004).
[37] Y. Fukuyama, Y. Moriwaki, and Y. Matsuo, Phys. Rev. A **75**, 032725 (2007).
[38] P. Moroshkin and K. Kono, Phys. Rev. A **93**, 052510 (2016).
[39] M. Mella and F. Cargnoni, J. Phys. Chem. A **118**, 6473 (2014).
[40] X. Zhang and M. Drabbels, J. Chem. Phys. **137**, 051102 (2012).
[41] D. Bonhommeau, P. T. Lake, Jr., C. L. Quiniou, M. Lewerenz, and N. Halberstadt, J. Chem. Phys. **126**, 051104 (2007).
[42] D. Bonhommeau, M. Lewerenz, and N. Halberstadt, J. Chem. Phys. **128**, 054302 (2008).
[43] S. Smolarek, N. B. Brauer, W. J. Burma, and M. Drabbels, J. Am. Chem. Soc. **132**, 14086 (2010).
[44] A. Leal *et al.*, J. Chem. Phys. **144**, 094302 (2016).
[45] D. Mateo *et al.*, J. Chem. Phys. **140**, 131101 (2014).
[46] W. H. Press, S. A. Teukolsky, W. T. Vetterling, and B. P. Flannery, *Numerical Recipes* (Cambridge University Press, Cambridge, 1992).
[47] J. J. Curry, J. Phys. Chem. Ref. Data **33**, 725 (2004).
[48] F. Cargnoni, A. Ponti, and M. Mella, Phys. Chem. Chem. Phys. **15**, 18410 (2013).
[49] R. A. Aziz, A. R. Janzen, and M. R. Moldover, Phys. Rev. Lett. **74**, 1586 (1995).
[50] Diagonalization gives the eigenvectors in increasing energy order, irrespective of their electronic character. We have imposed "adiabatic following" so that a given curve does not change label because of a crossing if it does not mix with another state at that point. It was implemented by (i) adding a negligibly small magnetic field to lift Kramer's degeneracy by a tiny amount and (ii) giving label k to a state at r_j if its scalar product with the eigenstate k at the previous distance r_{j-1} was at least equal to a critical value, taken here as 0.8. The reference order was taken at a distance where the states were in the "natural" order: $6\widetilde{S}$ (1 pair of states), $5\widetilde{D}$ (5 pairs), and $6\widetilde{P}$ (3 pairs).
[51] M. S. Child, *Molecular Collision Theory* (Academic Press, 1974).
[52] R. B. Bernstein, *Atom-Molecule Collision Theory: A Guide for the Experimentalist* (Plenum Press, New York, 1979).
[53] F. R. Brühl, R. A. Trasca, and W. E. Ernst, J. Chem. Phys. **115**, 10220 (2001).
[54] L. Fechner, B. Grüner, A. Sieg, C. Callegari, F. Ancilotto, F. Stienkemeier, and M. Mudrich, Phys. Chem. Chem. Phys. **14**, 3843 (2012).
[55] F. Lackner, J. Poms, G. Krois, J. V. Pototschnig, and W. E. Ernst, J. Phys. Chem. A **117**, 11866 (2013).
[56] E. Loginov and M. Drabbels, J. Phys. Chem. A **118**, 2738 (2014).
[57] D. G. Truhlar, J. Comput. Phys. **10**, 123 (1972).
[58] J. W. Cooley, Math. Comput. **15**, 363 (1961).
[59] W. Lester, J. Comput. Phys. **3**, 322 (1968).
[60] W. Lester, Methods Comput. Phys. **10**, 211 (1971).
[61] J. S. Coursey, D. J. Schwab, J. J. Tsai, and R. A. Dragoset, Atomic weights and isotopic composition, NIST database, http://www.nist.gov/pml/data/comp.cfm.
[62] H. Karlsson and U. Litzén, Phys. Scr. **60**, 321 (1999).
[63] A. Kramida, Yu. Ralchenko, J. Reader, and NIST ASD Team, NIST Atomic Spectra Database (version 5.3), available: http://physics.nist.gov/asd, 14 January 2017, National Institute of Standards and Technology, Gaithersburg, MD, 2015 (online).
[64] From A_{ul} Einstein coefficients in Ref. 47, 2017.
[65] S. L. Fiedler, D. Mateo, T. Aleksanyan, and J. Eloranta, Phys. Rev. B **86**, 144522 (2012).
[66] A. Leal, D. Mateo, A. Hernando, M. Pi, M. Barranco, A. Ponti, F. Cargnoni, and M. Drabbels, Phys. Rev. B **90**, 224518 (2014).
[67] R. Batulin, P. Moroshkin, D. A. Tayurskii, and K. Kono, AIP Adv. **8**, 015328 (2018).
[68] G. Katzer, Character table for the D$_{7h}$ point group, http://gernot-katzers-spice-pages.com/character_tables/D7h.html, 2017.
[69] M. Leino, A. Viel, and R. E. Zillich, J. Chem. Phys. **134**, 024316 (2011).
[70] F. Coppens, J. von Vangerow, M. Barranco, N. Halberstadt, F. Stienkemeier, M. Pi, and M. Mudrich, Phys. Chem. Chem. Phys. **20**, 9309 (2018).